Structural Engineering and Mechanics, Vol. 18, No. 2 (2004) 247-262
DOI: http://dx.doi.org/10.12989/sem.2004.18.2.247

A non-symmetric non-periodic B3-spline finite strip method

Kyeong-Ho Kim†

Chungsuk Engineering Specific, Structural Division, 57 Karak-dong, Songpa-gu, Seoul, Korea

Chang-Koon Choi‡

Department of Civil and Environmental Engineering, KAIST, Daejeon 373-1, Korea

(Received October 10, 2003, Accepted March 23, 2004)

Abstract. In the earlier application of the spline finite strip method(FSM), the uniform B3-spline functions were used in the longitudinal direction while the conventional interpolation functions were used in the transverse direction to construct the displacement filed in a strip. To overcome the shortcoming of the uniform B3-spline, non-periodic B-spline was developed as the displacement function. The use of non-periodic B3-spline function requires no tangential vectors at both ends to interpolate the geometry of shell and the Kronecker delta property is also satisfied at the end boundaries. Recently, non-periodic spline FSM which was modified to have a multiple knots at the boundary was developed for the shell analysis and applied to the analysis of bridges. In the formulation of a non-symmetric spline finite strip method, the concepts of non-periodic B3-spline and a stress-resultant finite strip with drilling degrees of freedom for a shell are used. The introduction of non-symmetrically spaced knots in the longitudinal direction allows the selective local refinement to improve the accuracy of solution at the connections or at the location of concentrated load. A number of numerical tests were performed to prove the accuracy and efficiency of the present study.

Key words: non-periodic B-spline function; stress-resultant shell; a non-symmetric spline finite strip method.

1. Introduction

As the finite strip method(FSM) uses a higher-order polynomials in the longitudinal direction, it is possible to analyze a type of structures, such as box girder bridges, using a smaller number of degrees of freedom in comparison with the finite element method. These finite strip methods can be categorized into (1) the semi-analytical finite strip method and (2) the spline finite strip method according to the function type used for its formulation. The semi-analytical finite strip method uses a trigonometric function series in the longitudinal direction which satisfy the end conditions of a strip a priori and simple polynomials in the other direction. However, the use of trigonometric

† Director
‡ Institute Chair Professor

function series is disadvantageous when used for the problems where the derivatives of the function are required to be discontinuous since the trigonometric function series are continuously differentiable. On the other hand, the spline functions do not have this problem and moreover, a suitable spline function with the required continuity(or discontinuity) conditions can be always found (Cheung 1983). When the uniform B3-splines are used for the isoparametric spline finite strip method, the shape function does not satisfy the Kronecker delta properties at the end boundary. Therefore, the special treatments such as the modified B3-splines and transformation method are required to satisfy the boundary conditions (Cheung *et al.* 1993, 1995). As a treatment of this problem, the non-periodic B3-spline for description of both the displacement and the geometry was introduced (Cheung *et al.* 2001). The two major advantages of non-periodic B-splines are that the additional information such as the end tangential vectors is not required to define the geometry of shell and that the shape function satisfies the Kronecker delta properties at the end boundary. In spite of these advantages, since all the nodes in the strip formulated based on non-periodic splines are equally spaced along the longitudinal direction, there are some limitations for local refinement which is necessary for the accurate stress evaluation at the locations of concentrated or patch loading, abrupt changes of geometry and material properties, internal supports, etc..

The main purpose of this study is to develop a non-symmetric spline finite strip method for the effective solution to the problem that the interior nodes of the strip are not regurarly spaced along the longitudinal direction. The finite strip element proposed in this study has non-symmetrically spaced interior nodes in the longitudinal direction of strip that is efficient to generate locally dense node distribution for the analysis of the stresses at the locations where the high stress concentration exists.

The efficiency and accuracy of the proposed method are demonstrated through a series of numerical examples.

2. Non-periodic B-splines

The basic spline curves can be represented in terms of B-spline functions as

$$p(x) = \sum_{i=-1}^{n+1} \alpha_i \phi_{i,k}(x) \tag{1}$$

where $p(x)$ is a spline curve and $\phi_{i,k}$ represents the i-th B-spline function of order k. α_i is a set of control points (or parameters) which are the curve defining vector.

The i-th B-spline function $\phi_{i,k}$ is defined by the following recursive equation

$$\phi_{i,k}(x) = \begin{cases} 1 & \text{for } x_i \le x \le x_{i+1} \\ 0 & \text{otherwise} \end{cases} \tag{2a}$$

and

$$\phi_{i,k}(x) = \frac{(x - x_i)}{(x_{i+k-1} - x_i)} \phi_{i,k-1}(x) + \frac{(x_{i+k} - x)}{(x_{i+k} - x_{i+1})} \phi_{i+1,k-1}(x) \tag{2b}$$

where the knot vector is $(x_i, ..., x_{i+k})$.

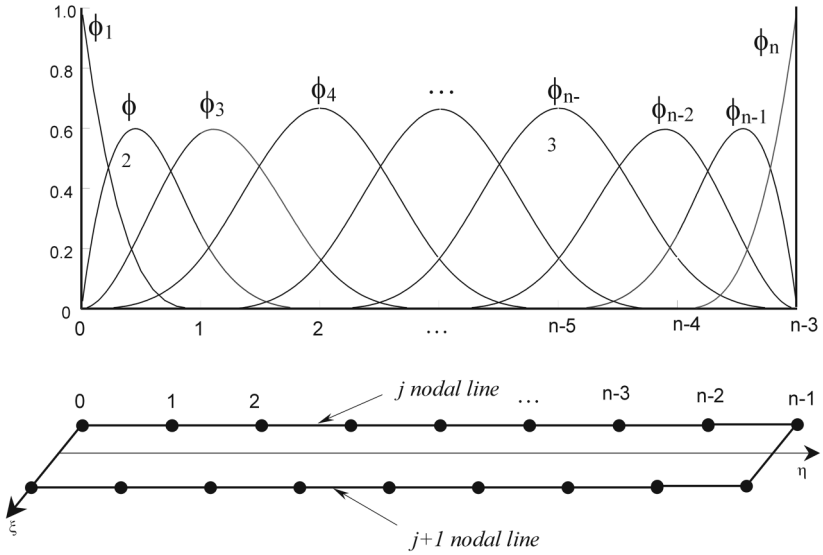

Fig. 1 Non-periodic B3-spline series in strip element

The non-periodic B-spline function is defined by the recursive form expressed as Eq. (2). For example, if B3-spline series has repeated knot vector values at the boundary (end) point, the extra sections beyond the end points have all zero lengths, and thus both initial and final knots become multiple knots with a multiplicity of 4 which is equal to the order of B3-spline. In the non-periodic B3-spline series as shown in Fig. 1, the use of multiple knots at the boundary enables that the Kronecker delta property is satisfied and thus the real values of the field variables, not parameters, can be directly obtained at the boundary. Therefore, the boundary conditions can be treated more easily than the periodic B-spline function (Cheung *et al.* 2001).

3. Formulation of shell strip with non-symmetrically spaced nodes

To define the geometry of strip and local axis, a resultant stress shell is divided into several strips first. The formulation of stiffness matrix and the load vector of a strip is based on six degrees of freedom per node i.e., three independent rotational DOFs, θ_x, θ_y, θ_z and three translational DOFs, u, v, w (Fig. 2). A non-periodic B3-spline and a stress-resultant finite strip with drilling degrees of freedom for a shell were employed in this study (Hong 2001). The non-symmetric finite strip has non-symmetrical numbers of sections and nodes in two nodal lines which define a curve defining polygon of an arbitrary number of vertices.

In this study, the geometry of the C^0 degenerated shell strip is defined in terms of functions of mid-surface.

$$x = \sum_{i=1}^{n} \sum_{j=1}^{2} N_{ij}(\xi, \eta)\boldsymbol{q}_{ij} + t\boldsymbol{V}_t \tag{3}$$

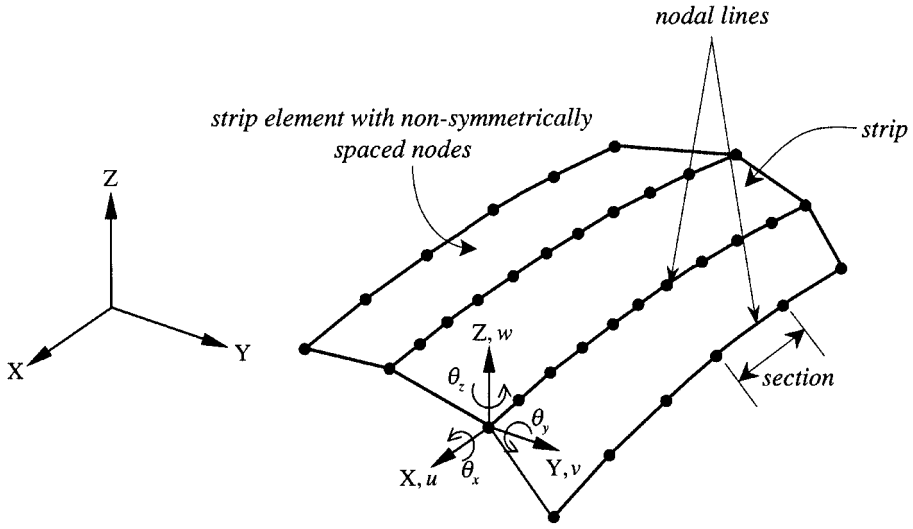

Fig. 2 Strip geometry and coordinates system

where

$$N_{ij}(\xi, \eta) = L_j(\xi)\phi_{i,4}(\eta) \tag{4}$$

and where V_t is the unit vector normal to the shell mid-surface at each integration point, t is the linear coordinate in the range $-h/2 < t < h/2$ in the normal-to-mid-surface direction and h is the thickness at the integration point. $\boldsymbol{x} = (x, y, z)$ and $\boldsymbol{q_{ij}} = (x, y, z)_{ij}$ are the i-th curve defining vectors of the j-th nodal line of the strip. L_j is the linear Lagrangian polynomial and $\phi_{i,4}$ is the non-periodic B3-spline function. The definitions of displacement and strain field can be found in the previous study of authors (Choi *et al.* 2001).

To obtain the element stiffness matrix for elastic analysis, the total potential energy of the shell strip is given by

$$\Pi = \frac{1}{2}\int(\boldsymbol{\varepsilon}_m^T\boldsymbol{D}_m\boldsymbol{\varepsilon}_m + \boldsymbol{\varepsilon}_b^T\boldsymbol{D}_b\boldsymbol{\varepsilon}_b + \boldsymbol{\varepsilon}_s^T\boldsymbol{D}_s\boldsymbol{\varepsilon}_s)dA - W \tag{5}$$

where W is the potential energy of applied load and the rigidity matrices D_m, D_b, D_s are associated with the membrane, bending, and transverse shear strain, respectively.

By the principle of stationary potential energy for equilibrium, the membrane, bending, shear, and drilling rotational contribution to the material stiffness matrix is derived as

$$\boldsymbol{K} = \boldsymbol{K}_m + \boldsymbol{K}_b + \boldsymbol{K}_s + \boldsymbol{K}_\theta = \int\boldsymbol{B}_m^T\boldsymbol{D}_m\boldsymbol{B}_m dA + \int\boldsymbol{B}_b^T\boldsymbol{D}_b\boldsymbol{B}_b dA + \int\boldsymbol{B}_s^T\boldsymbol{D}_s\boldsymbol{B}_s dA + \Phi Gh\int\boldsymbol{B}_\theta^T\boldsymbol{B}_\theta dA \tag{6}$$

The strain by the drilling DOFs associated with the in-plane rotation of the mid-surface can be expressed as (Choi *et al.* 2003).

$$\varepsilon_\theta = \theta_t - 1/2(u_{s,r} - u_{r,s}) = 0 \tag{7}$$

where θ_t is the drilling rotation of shell mid-surface in the local coordinate systems. The potential energy of the shell strip derived by the drilling DOFs is given as

$$\Pi_\theta = \Phi G h \frac{1}{2}\int \varepsilon_\theta^T \varepsilon_\theta dA \tag{8}$$

And the rotational stiffness matrix can be expressed as

$$\boldsymbol{K}_\theta = \Phi G h \frac{1}{2}\int \boldsymbol{B}_\theta^T \boldsymbol{B}_\theta dA \tag{9}$$

where

$$\boldsymbol{B}_\theta = \left[\frac{1}{2}(\overline{N}_{,s}^I \boldsymbol{V}_r^T - \overline{N}_{,r}^I \boldsymbol{V}_s^T) N^I \boldsymbol{V}_t^T\right] \tag{10}$$

where Φ is the penalty constant which has only a minimum influence on the results of plane problems. However, an inappropriate choice of Φ may result in erroneous solution for structures with curved geometry (Chroscielewski *et al.* 1997). Since there is no precise method to decide the value of Φ, the value of Φ is chosen to be 1.0 based on the numerical experiments performed by previous study of authors (Hong 2001).

In computing strip matrices, the selectively reduced integration scheme is used which is also helpful to avoid shear locking (Zienkiewicz *et al.* 1971). Table 1 gives the selectively reduced integration rule for linear shell strip. The integration rule is given as the number of rows of Gaussian points in the ξ direction by the corresponding number in the η direction in each section.

When the reduced integration scheme is used in evaluating the stiffness of drilling part to avoid the over-constrained situation similar to the shear locking, five spurious zero-energy modes which cause the singularity problem may be invoked if the strips are coplanar (Choi *et al.* 2001, 2002, Kim 2003, Kebari *et al.* 1991). Therefore, the selectively reduced integration scheme is adopted only for computing shear stiffness in this study. Thus, the number of zero energy modes invoked by the selectively reduced integration can be reduced to one. Moreover, this zero energy mode is non-communicable and therefore it can be removed when at least two strips are used together (Cheung *et al.* 2001).

Table 1 Integration rules

Stiffness	Membrane stiffness	Bending stiffness	Shear stiffness	Drilling stiffness	Zero energy modes
Selectively reduced	2×4	2×4	1×3	2×4	1^*

* : Non communicable mode

4. Integration method for a strip with non-symmetrically spaced nodes

Fig. 3(a) shows the conventional finite strip element which has symmetrically spaced nodes in both nodal lines. The non-symmetric spline finite strip element proposed in this study is also shown in Fig. 3(b). This non-symmetric spline finite strip element can be effectively applied for the selective local refinement to obtain more accurate results in the region of high stress concentration.

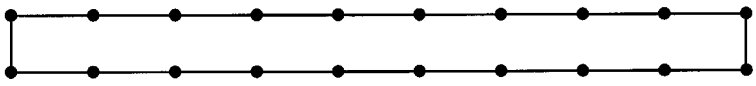

(a) Conventional strip element

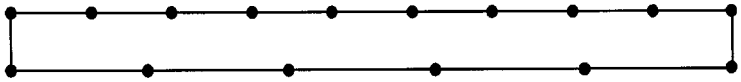

(b) A non-symmetric spline finite strip element

Fig. 3 Strip element

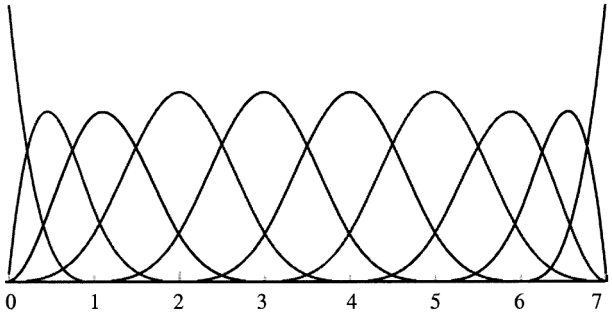

(a) Ten non-periodic B3-splines with eight knots value

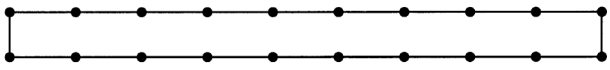

(b) Single linear strip with ten interior nodes(nine sections)

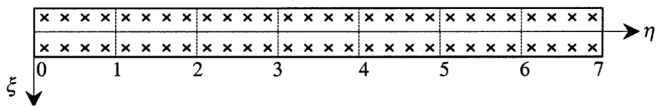

(c) Full integration points of a strip with seven sections (seven segments)

Fig. 4 Numerical integration points of strip

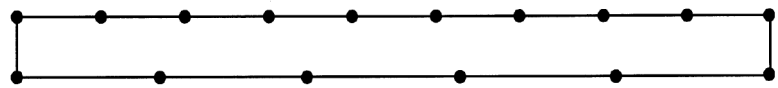

(a) A non-symmetric spline finite strip element

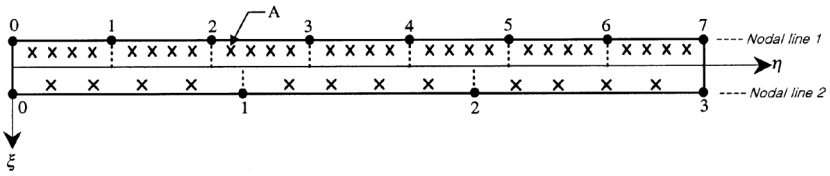

(b) Integral scheme for each nodal line

Fig. 5 Integration method for non-symmetric spline finite strip element

As shown in Fig. 4, a single strip with ten symmetric interior nodes in the longitudinal direction has seven sections (or segments) and the numerical integration to compute the strip stiffness is carried out within each section (Hong 2001). However, in the non-symmetric spline finite strip element shown in Fig. 5(a), the two nodal lines have different numbers of nodes, and therefore, the number of sections to be integrated are different for two nodal lines. Thus integration should be performed for each nodal line first and then results for both nodal lines can be combined to form the stiffness of entire strip as shown in Fig. 5(b).

In order to calculate the Jacobian matrix for the stiffness matrix of a strip, the spline function and its derivative values should be estimated at each Gauss point within each section along the both nodal lines. In the conventional symmetric spline finite strip element, the number of nodes on two nodal lines and also the numbers of sections are same. The global positions of knots in a strip can be established in order that the largest knot number should be same to the number of sections to be integrated. Therefore, the spline function and its derivative values can be obtained by transforming the local coordinates of the Gauss points in each section into the corresponding global knot values. However, since the numbers of nodes on two nodal lines are different from each other in the non-symmetric spline finite strip element, a new method to obtain the spline function and its derivative values at each Gauss point is necessary. The mapping and unit normalization at the two nodal lines are the basic ideas of the new method proposed in this study. The method is outlined as follows (Fig. 6) (Kim 2003).

1) Transform the local coordinates of Gauss points $(-1 \le \xi \le 1)$ in each section into the corresponding values of knots in global system which range from 0 to the number of sections to be integrated in two nodal lines as

$$t_1 = \frac{(\xi + 1)}{2} + (nsect1 - 1)$$

$$t_2 = \frac{(\xi + 1)}{2} + (nsect2 - 1) \tag{11}$$

where ξ : Local coordinates of Gauss point $(-1 \le \xi \le 1)$

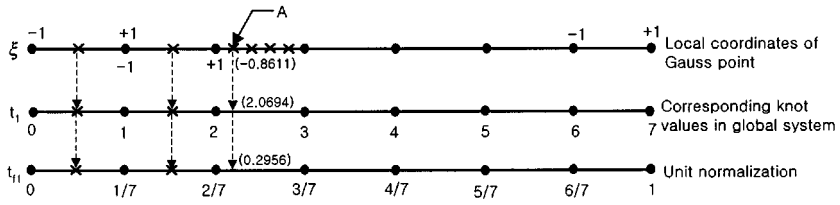

(a) Mapping of integral points in nodal line 1

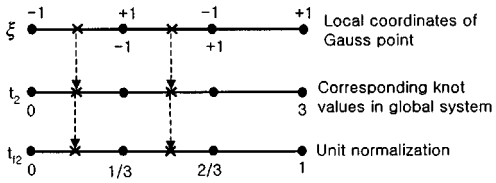

(b) Mapping of integral points in nodal line 2

Fig. 6 Precise mapping method for each nodal line

For example, the local coordinate of the first Gauss point of the third section on the upper nodal line in Fig. 6 (point A between knots 2 and 3) $\xi = -0.861$ becomes $t_1 = 2.0694$ in the global system.

2) Normalize the transformed Gauss point in two nodal lines in the global system as

$$t_{f1} = t_1 \times \frac{1}{nsect1}$$

$$t_{f2} = t_2 \times \frac{1}{nsect2} \tag{12}$$

where *nsect* 1 : Number of sections to be integrated for nodal line 1
nsect 2 : Number of sections to be integrated for nodal line 2

The value of 2.0694 in the above example is now divided by the number of sections to be integrated in the nodal line 1, (i.e., 7) to obtain the normalized local coordinates of point A as 2.0694/7 = 0.2956.

3) Evaluate the shape function and its derivative values at each normalized Gauss point as following

$$N_{ij}(\xi, \eta) = L_j(\xi)\phi_{i,k}(\eta) \tag{13}$$

$$\frac{\partial N_{ij}}{\partial \xi} = \phi_{i,k}\frac{\partial L_j}{\partial \xi}$$

$$\frac{\partial N_{ij}}{\partial \eta} = L_j\frac{\partial \phi_{i,k}}{\partial \eta} \tag{14}$$

$$\phi_{i,k}(t) = \frac{(t-T_i)}{(T_{i+k-1}-T_i)}\phi_{i,k-1}(t) + \frac{(T_{i+k}-t)}{(T_{i+k}-T_{i+1})}\phi_{i+1,k-1}(t) \tag{15}$$

$$\frac{\partial \phi_{i,k}^{(j)}(t)}{\partial \eta} = (k-1)\ldots(k-j)\left(\frac{\phi_{i,k-1}^{(j-1)}(t)}{T_{i+k-1}-T_i} + \frac{\phi_{i+1,k-1}^{(j-1)}(t)}{T_{i+k}-T_{i+1}}\right) \tag{16}$$

where (j) denotes the order of derivatives.

Since the value of Gauss point is normalized, the B3-spline function should be generated by normalizing knots in two nodal lines as shown in Fig. 7.

4) Calculate the Jacobian matrix J, its determinant and the Cartesian derivatives of the shape function as following relation.

$$\begin{bmatrix} \frac{\partial N_{ij}}{\partial x} \\ \frac{\partial N_{ij}}{\partial y} \end{bmatrix} = \begin{bmatrix} \frac{\partial \xi}{\partial x} & \frac{\partial \eta}{\partial x} \\ \frac{\partial \xi}{\partial y} & \frac{\partial \eta}{\partial y} \end{bmatrix} \begin{bmatrix} \frac{\partial N_{ij}}{\partial \xi} \\ \frac{\partial N_{ij}}{\partial \eta} \end{bmatrix} \tag{17}$$

5) Estimate the stiffness of a non-symmetric spline finite strip element by using the Jacobian matrix.

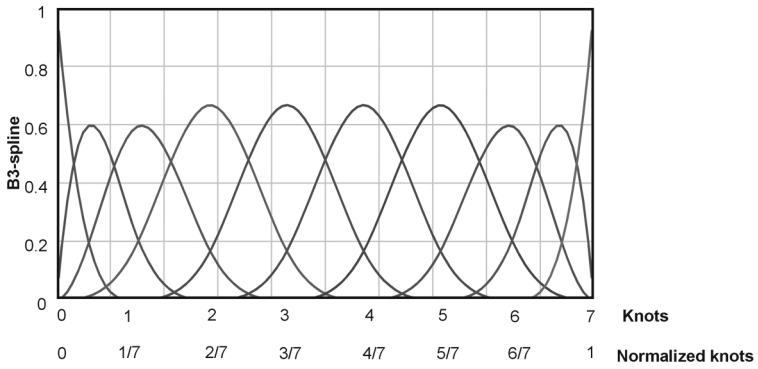

(a) B3-spline for normalized knots in nodal line 1

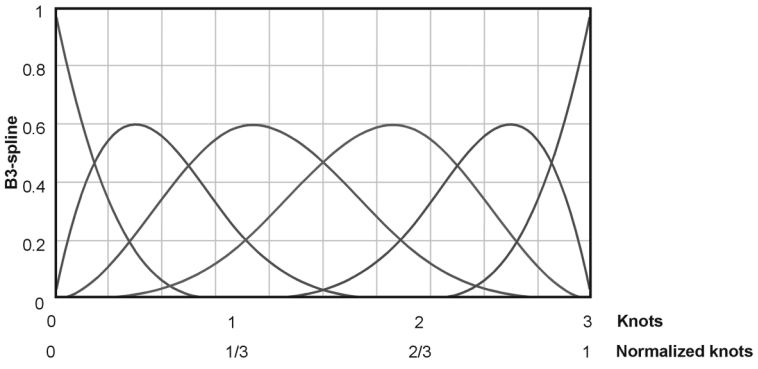

(b) B3-spline for normalized knots in nodal line 2

Fig. 7 B3-spline for normalized knots for each nodal line

5. Numerical examples

5.1 Cantilever box

The cantilever box with a length of 10.0 m was analyzed to examine the basic behavior of spline FSM with non-symmetrically spaced interior nodes (Kim 2003). As shown in Fig. 8(a), the cantilever beam is clamped at one end and free at the other end. The elastic modulus and Poisson's ratio used for the analysis are 2×10^6 t/m^2 and 0.0, respectively. The shape of cross-section of the beam and strip divisions are shown in Fig. 8(b). The beam is subjected to two load conditions, i.e., two vertical unit loads at the free end of the box and two unit loads acting in the opposite direction to generate twisting force at the end.

Two models were selected as shown in Fig. 9 for the comparison purpose. Model 1 is the strip element with symmetric nodes and model 2 is the strip element with non-symmetric nodes which is more refined at the four corner connections. Tests were carried out with two loading conditions for each model to illustrate the efficiency of spline FSM with non-symmetrically spaced knots. Test

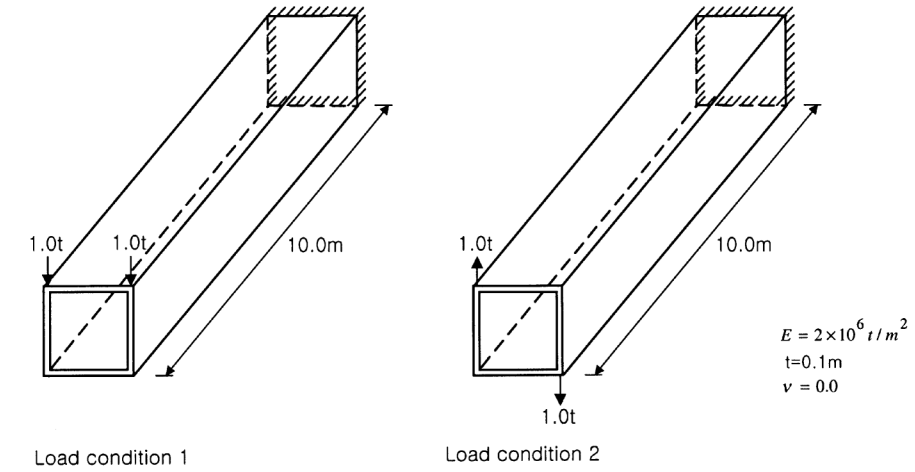

(a) Cantilever box

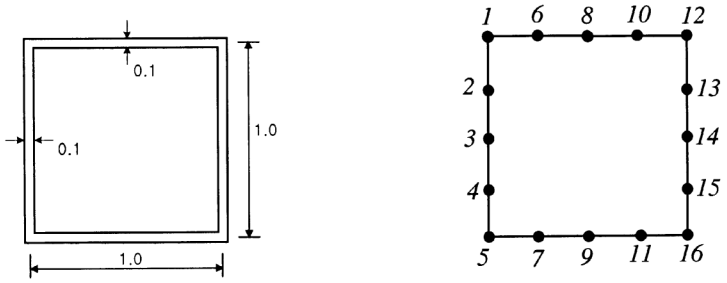

(b) Cross-section and strip division

Fig. 8 Cantilever box

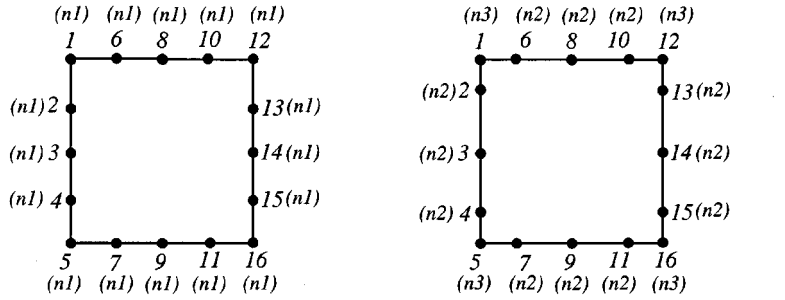

(a) Model 1: Symmetric node (b) Model 2: Non-symmetric node

*(n1, etc.): Number of nodes used in the longitudinal direction

Fig. 9 Analytical models

cases were summarized according to the number of nodes used in the longitudinal direction (Table 2). The total degrees of freedom were maintained same for symmetric and non-symmetric models during the tests.

Table 2 Analytical cases

Test cases	Models	Nodes on nodal line			Degrees of freedom	Remarks
		*n*1	*n*2	*n*3		
Case 1	Symmetric	5	-	-	480	Coarse mesh
	Non-symmetric	-	4	8		
Case 2	Symmetric	11	-	-	1056	Fairly refined mesh
	Non-symmetric	-	9	17		
Case 3	Symmetric	21	-	-	2016	Refined mesh
	Non-symmetric	-	16	36		
Case 4	Symmetric	31	-	-	2976	More refined mesh
	Non-symmetric	-	27	43		

Table 3 Deflection at free end (Load condition 1)

(unit :$\times 10^{-2}$ cm)

	Vertical displacement				Normalized values			
Meshes / Models	Coarse mesh (480 dof)	Fairly refined mesh (1056 dof)	Refined mesh (2016 dof)	More refined mesh (2976 dof)	Coarse mesh (480 dof)	Fairly refined mesh (1056 dof)	Refined mesh (2016 dof)	More refined mesh (2976 dof)
Symmetric	0.51049	0.51145	0.51185	0.51193	0.9972	0.9991	0.9998	1.0000
Non-symmetric	0.51131	0.51185	0.51189	0.51194	0.9988	0.9998	0.9999	1.0000
FEM (15552 dof) (FESA [9])	0.51194				1.0000			

Table 4 Twisting at free end (Load condition 2)

($\times 10^{-3}$)

	Twisting				Normalized values			
Meshes / Models	Coarse mesh (480 dof)	Fairly refined mesh (1056 dof)	Refined mesh (2016 dof)	More refined mesh (2976 dof)	Coarse mesh (480 dof)	Fairly refined mesh (1056 dof)	Refined mesh (2016 dof)	More refined mesh (2976 dof)
Symmetric	0.22691	0.23696	0.24060	0.24158	0.9376	0.9792	0.9942	0.9982
Non-symmetric	0.23301	0.23893	0.24103	0.24158	0.9629	0.9873	0.9960	0.9983
FEM (15552 dof) (FESA [9])	0.24200				1.0000			

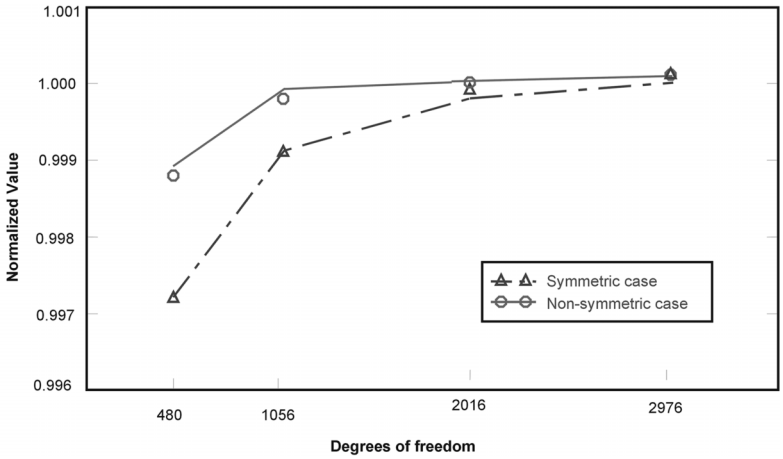

(a) Deflection at free end (Load condition 1)

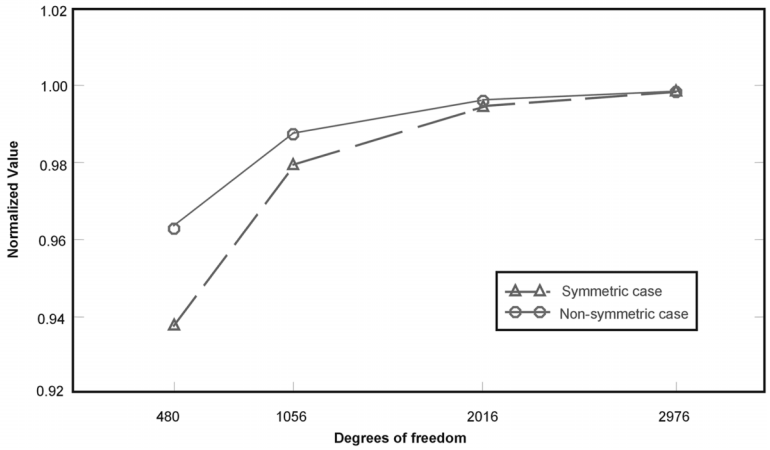

(b) Twisting at free (Load condition 2)

Fig. 10 Convergence Curve

The numerical results for each load condition are presented in Table 3 and Table 4, together with the reference values by FEM. Table 3 shows the vertical displacement and its normalized values at free end for two models. Table 4 presents the twisting and its normalized values of box, computed by considering the relative displacement of box section at free end. The convergence curves for two models are presented in Fig. 10. As shown in these figures, the more improved results are obtained by the non-symmetric spline strip element than those by the symmetric spline strip element.

5.2 Fam and Turkstra's curved box girder bridge

The structure shown in Fig. 11 is a plexiglass model studied extensively by Fam and Turkstra (Fam *et al.* 1975, 1976). The elastic modulus and Poisson's ratio are 400,000 psi and 0.36 respectively. The supports are modeled as rigid diaphragms, where no vertical movements are permitted. The bridge model is circularly curved in plan with a centerline radius of 51 in. The girder is subjected to a single concentrated load of 20 lb at midspan over the outer web.

The analytical modeling for transverse and longitudinal direction is shown in Fig. 12 in which the entire bridge is divided into 20 strips. The smaller strip widths were used near the box corners due to the high stresses and steep stress gradients at the box corner. In the symmetric spline FSM, all strips are divided into 18 equal sections in the longitudinal direction. However, in non-symmetric spline FSM, meshes are refined by the means of non-symmetric knot spacing at the location of concentrated load as shown in Fig. 12.

The results were compared with those of Fam and Turksta's experiment and their finite element analysis. The vertical displacements of the top flange at the location of the interior and exterior webs for half span are shown in Fig. 13. The transverse distribution of longitudinal membrane stress at midspan is shown in Fig. 14. As can be seen in these figures, the spline FSM with non-symmetrically spaced knots can pick up the peak stress values at the location of concentrated load more accurately.

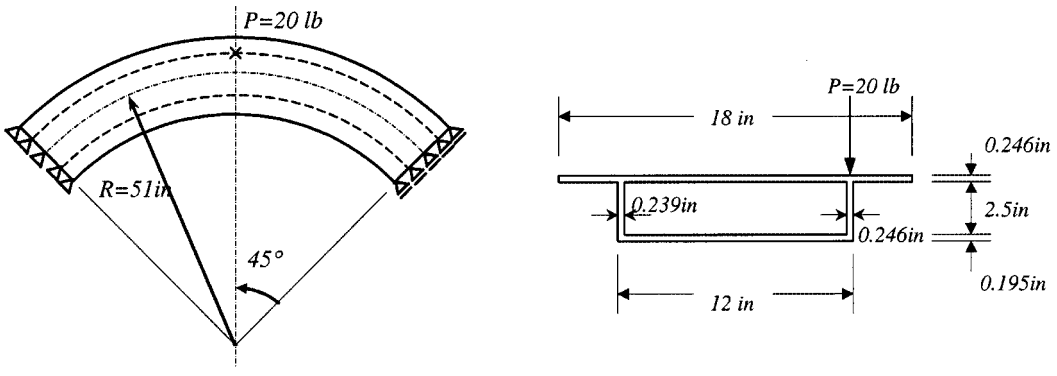

(a) Plan geometry of bridge model (b) Typical section dimensions

Fig. 11 Geometry and section dimensions for Fam and Turkstra's model

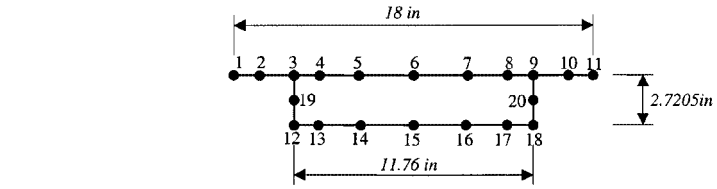

(a) Analytical model of cross-section

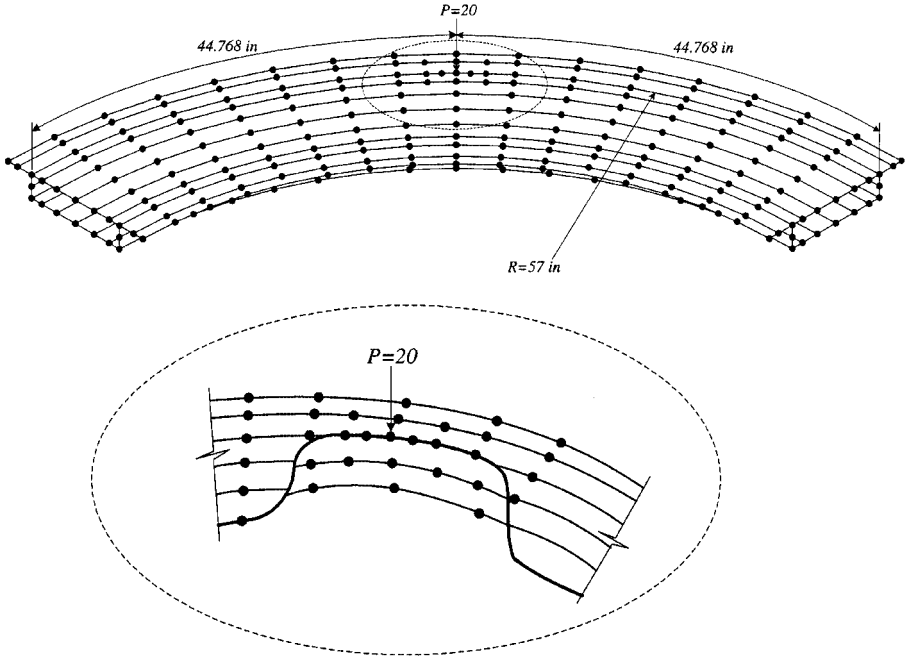

(b) Strip division

Fig. 12 Analytical model

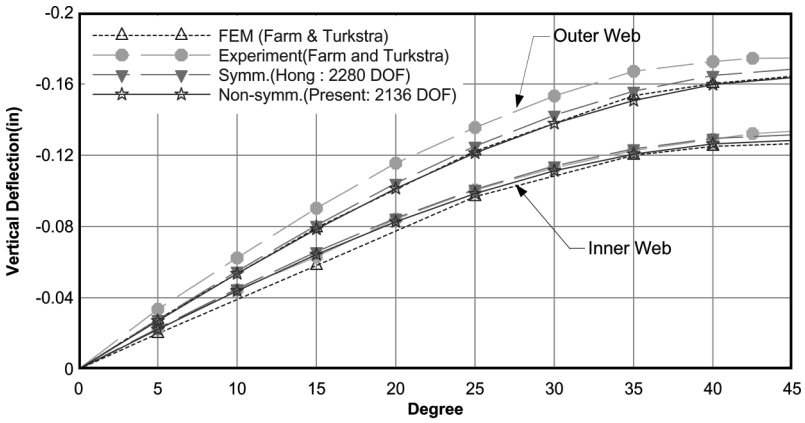

Fig. 13 Vertical displacement of flange for half span

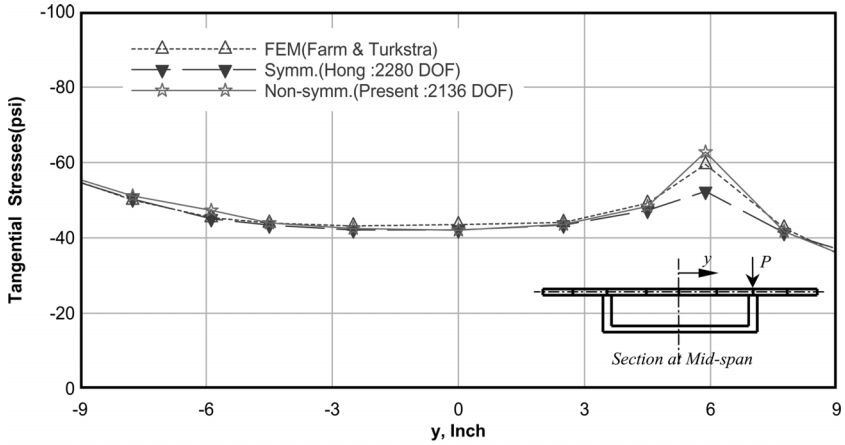

(a) Upper flange

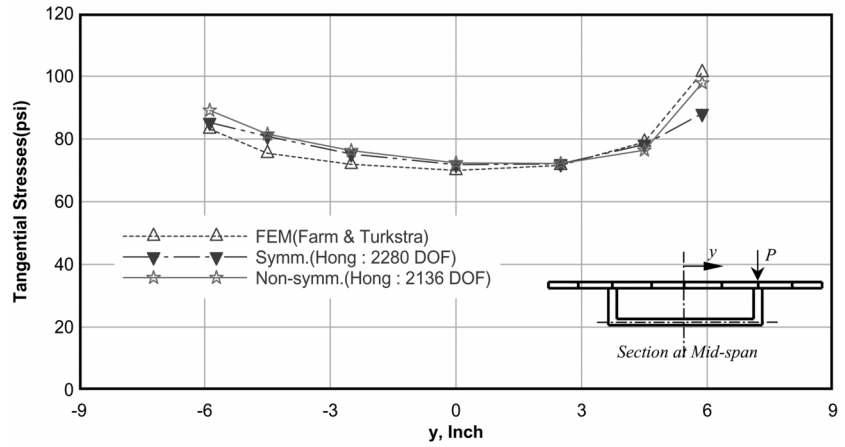

(b) Lower flange

Fig. 14 Longitudinal membrane stress at midspan

6. Conclusions

A non-symmetric spline finite strip method is presented in this study. This has been achieved based on the extension of authors' previous studies that are the non-periodic B3-spline and a stress-resultant finite strip with drilling degrees of freedom for a shell strip. The development of the non-symmetrically spaced interior nodes in the longitudinal direction of strip can generalize the concept of non-periodic B-spline FSM and improve the accuracy of the stress evaluation in the region of high stress gradients by generating locally dense node distribution. As can be seen from the numerical examples, the introduction of non-symmetrically spaced nodes makes it possible to generate the selective local refinement to improve the accuracy of solution in the region of stress concentration that may not be possible with the conventional symmetrically spaced strip.

More improved results were obtained by the non-symmetric B3-spline finite strip method compared with those obtained by other solutions for various structures.

Acknowledgements

This work has been supported in part by SisTeC (Smart Infra-structure Technology Center) which is funded by Korea Science and Engineering Foundation. The first author would like to acknowledge their financial support to this research.

References

Au, F.T.K and Cheung, Y.K. (1993), "Isoparametric spline finite strip for plane structures", *Comput. Struct.*, **48**(1), 23-32.

Cheung, Y.K. (1983), "Static analysis of right box girder bridges by spline finite strip method", *Proc. the Institution of Civil Engineers*, Part 2, 75, June, 311-323.

Cheung, Y.K. and Au, F.T.K. (1995), "Isoparametric spline finite strip for degenerated shells", *Thin-Walled Structures*, **21**, 65-92.

Choi, C.K. and Hong, H.S. (2001), "Finite strip analysis of multi-span box girder bridges by using non-periodic B-spline interpolation", *Struct. Eng. Mech.*, **12**(3), 313-328.

Choi, C.K., Hong, H.S. and Kim, K.H. (2003), "Unequally spaced non-periodic B-spline finite strip method", *Int. J. Numer. Meth. Eng.*, **57**, 35-55.

Choi, C.K., Kim, K.H. and Hong, H.S. (2002), "Spline finite strip analysis of prestressed concrete box-girder bridges", *Eng. Struct.*, **24**(12), 1575-1586

Chroscielewski, J., Makowski, J. and Stumpf, H. (1997), "Finite element analysis of smooth, folded and multi-shell structure", *Comput. Meth. Appl. Mech. Eng.*, **141**, 1-46.

Fam, A.R.M. and Turkstra, C. (1975), "A finite element scheme for box bridge analysis", *Comput. Struct.*, **5**, 179-186.

Fam, A.R.M. and Turkstra, C. (1976), "Model study of horizontally curved box girder", *J. Struct. Div.*, ASCE, ST5, 1097-1108.

Hong, H.S. (2001), "A study on the development of shell strip by non-periodic B-spline finite strip method and application to bridge analysis", Ph.D. Dissertation, Department of Civil and Environmental Engineering, KAIST.

Ibrahimbegovic, A., Taylor, R.L. and Wilson, E.L. (1990), "A robust quadrilateral membrane finite element with drilling degree of freedom", *Int. J. Numer. Meth. Eng.*, **30**, 445-457.

Kebari, H. and Cassell, A.C. (1991), "Non-conforming modes stabilization of a nine-node stress-resultant degenerated shell element with drilling freedom", *Comput. Struct.*, **40**(3), 569-580.

Kim, K.H. (2003), "A non-symmetric·non-periodic B3-spline spline finite strip element and its application to bridge analysis", Ph.D. Dissertation, Department of Civil and Environmental Engineering, KAIST.

Structural System Lab. (1998), KAIST. FESA. *User's Manual.*

Zienkiewicz, O.C., Taylor, R.L. and Too, J.M. (1971), "Reduced integration technique in general analysis plates and shells", *Int. J. Numer. Meth. Eng.*, **3**, 275-290.